Influence of Ion Size and Charge in Ion Transfer Processes Across a Liquid|Liquid Interface

Pedro Alexandrino Fernandes, M. Natália D. S. Cordeiro,* and José A. N. F. Gomes

CEQUP/Department Química, Faculdade de Ciências da Universidade do Porto, Rua do Campo Alegre 687, 4069-007 Porto, Portugal

Received: August 25, 1999; In Final Form: December 15, 1999

In this work, molecular dynamics simulations have been used to study the transfer of some alkaline ions (Na^+, K^+, and Rb^+), an alkaline-earth ion (Sr^{2+}), and an organic ion ($N(CH_3)_4^+$) across the water/2-heptanone liquid/liquid interface. Potentials of mean force were calculated and the ion transfer mechanisms were analyzed. The computed free energies of transfer exhibit a clear dependence on the ionic size and charge. In clear agreement with the experimental results obtained for several liquid/liquid biphasic systems, the free energies of transfer increase with the ionic charge and decrease with the ionic size. In all cases investigated, the potential of mean force for the transfer shows a monotonic increase in the Gibbs free energy as the ion progresses into the organic liquid. The major increase of the free energy occurs when the ion is on the organic side of the interface. The transfer seems to be an activationless process because there is no free energy barrier, this is true even in the case of the transfer of the organic ion. The transfer mechanism involves the formation of a water finger that connects the ions in the organic phase to the water phase during the transfer in both directions (i.e., from water to the organic phase and vice versa). For the organic and the alkaline ions, the water finger may be as long as 10 Å and, for the alkaline-earth ion, as long as 14 Å. In addition, it has been found that all the ions drag a part of their hydration shell into the organic phase, a phenomenon well documented experimentally. For similar ions, the number of water molecules and the fraction of the hydration shell dragged into the organic phase increased with the robustness of their shell. The $N(CH_3)_4^+$ ion drags slightly more water molecules than the alkaline ions, although the fraction of its hydration shell that remains in the organic solvent is much smaller. The mechanisms of the ion transfer processes studied here are all qualitatively similar, showing however a quantitative dependence on the ionic size and charge.

I. Introduction

Solvation and chemical reactivity at liquid interfaces plays a major role in many areas of chemistry, physics, and biology. Ion transfer across the interface between immiscible liquids is essential to processes such as phase-transfer catalysis, the kinetics of ion extraction, drug delivery problems in pharmacology, electrochemical sensors, or selective electrodyalisis.[1−3] Understanding the behavior of solutes and their reactivity at liquid interfaces is also extremely important at the fundamental/theoretical level because inhomogeneous media are characterized by a number of unique properties that are expected to influence the behavior of chemically active species in a way significantly different from that of bulk liquid or gas phase. Since the beginning of the century, several experimental and theoretical studies have been devoted to interfacial phenomena. However, despite the efforts of classical physical chemists, there is still an enormous lack of information about the microscopic properties of the interfaces or the ion-transfer mechanisms across them. In the past few years, however, the application of modern experimental techniques (like nonlinear optical spectroscopy)[4−9] has given new useful insights into interfacial systems. For instance, optical second harmonic generation together with sum frequency generation allowed the characterization of the molecular ordering of *n*-alkanes at the water/*n*-alkane interface. In a recent work of Mitrinovic et al.,[10] a new X-ray reflectivity technique was used to directly measure for the first time the width of a liquid/liquid interface. The value (3.3 ± 0.25 Å) obtained for the width of the water/hexane interface was shown to be in good agreement with the predictions from the capillary wave theory or from computer simulations. Molecular simulations methods, like Monte Carlo or molecular dynamics (MD), have contributed remarkably to our current microscopic understanding of interfacial systems.[11−16] In fact, a significant part of what is know about interfacial phenomena has been gathered by molecular simulation methods. These methods can provide the potential of mean force (PMF) governing the ion transfer[17−20] and the means to investigate the exchange of the solvation shell of the ion, which is the key step of the transfer process. Notice that even the newest experimental techniques are unable to describe these important features.

This work presents results of a series of MD simulations for the transfer of alkaline (Na^+, K^+, and Rb^+), alkaline-earth (Sr^{2+}), and organic ($N(CH_3)_4^+$) ions across the water/2-heptanone (HPT2) interface. The HPT2 solvent was chosen because it represents an important alternative to other commonly used organic solvents (e.g., 1,2-dichloroethane or nitrobenzene) that are highly toxic and, therefore, environmentally unnaceptable. HPT2, being nonaromatic and not halogenated, has a low toxicity and may thus be used in large-scale industrial processes. Also, recently, it has been demonstrated that HPT2 can be successfully applied in simple and assisted electrochemical ion transfers.[21,22] Alkaline, alkaline-earth, and the tetramethylamonium ions are among the most frequently used to perform experimental unnassisted electrochemical ion transfers.[23,24]

* Corresponding author. E-mail: ncordeir@fc.up.pt.

10.1021/jp993045z CCC: $19.00
Published on Web 02/17/2000

The microscopic characterization of the present liquid/liquid interface has been accomplished in an earlier work.[16] With this set of transfers, we are now able to examine the dependence of the energetics and mechanism of transfer on the size and charge of the ion. The transfer of the organic ion might shed some light on how the nature of the ion affects this phenomenon.

The outline of this paper is as follows. In Section II, the details of the simulations are briefly described. Then, in Section III, we discuss the results of the simulations, focusing on the PMFs of the ions transfers, the processes of the solvation shells exchange, the formation of the water fingers, and the water dragging effects. In addition, an attempt is made to clarify the dependence on the ion size and charge for this interfacial process by comparing the results obtained for the different ions. Finally, some concluding remarks are presented in the last section.

II. Simulation Details

A. Molecular Models and Potentials. The water molecules were described by the well-known SPC potential.[25]

The HPT2 molecules were modeled by united atom formalism with an eight-site interaction model. All bond lengths were kept fixed by applying the SHAKE algorithm.[26] The use of bond constraints allows us to increase the time step up to 2 fs when integrating the equations of motion. This increase results in a better exploration of the configurational space and, as previously checked, does not affect the simulation results. Flexible angles and dihedrals were considered by employing the CHARMm intramolecular force field.[27] The tetramethylamonium ion (TMA^+) was also modeled by united atom formalism, leading to a five-site interaction model. All intermolecular potentials are pairwise additive and include a Coulombic and a Lennard−Jones term. In summary, the total potential energy of the system, ($V_{total} = V_{intra} + V_{inter}$) was computed with eqs 1 and 2, with obvious notations, for the intra- and intermolecular interactions, respectively. One to four specific dihedral interactions were

$$V_{\text{intra}} = \sum^{\text{angles}} K_\theta(\theta - \theta^{\text{eq}})^2 + \sum^{\text{impropers}} K_{\text{impr}}(\theta_{\text{impr}} - \theta_{\text{impr}}^{\text{eq}})^2 + \sum^{\text{dihedrals}} K_{\text{dih}}(1 + \cos(m\theta_{\text{dih}} - \delta)) \quad (1)$$

$$V_{\text{inter}} = \sum^{\text{pairs}} \frac{q_i q_j}{r_{ij}} + \sum^{\text{pairs}} 4\epsilon_{ij}\left(\left(\frac{\sigma_{ij}}{r_{ij}}\right)^{12} - \left(\frac{\sigma_{ij}}{r_{ij}}\right)^{6}\right) \quad (2)$$

included as established in the CHARMm force field.

Atomic charges for HPT2 were obtained from quantum calculations as described previously.[28] All other atomic charges, as well as the parameters for the Lennard−Jones potentials were taken from the AMBER force field.[29] The Lennard−Jones parameters for the interactions between different species were derived using standard geometric combination rules; that is, $\sigma_{ij} = (\sigma_i\sigma_j)^{1/2}$ and $\epsilon_{ij} = (\epsilon_i\epsilon_j)^{1/2}$.

B. Method. *1. Simulated Systems.* The H_2O/HPT2 system was first represented by two independent boxes, one containing 794 water molecules and the other a mixture of 168 HPT2 molecules plus 15 water molecules. The latter box reproduces a solution of HPT2 saturated with water (8.3% H_2O (mol/mol)). Both boxes had initially the same cross section (25 × 25 Å) and lengths that mimic the experimental densities of the pure liquids ($\rho(H_2O) = 0.997$ g·cm^{-3} and $\rho(\text{HPT2}) = 0.8124$ g·cm^{-3}). After an individual equilibration of each box, they were joined together along their cross sections, and the interactions between the molecules of the two liquids were slowly switched on. During this process, the volume of the boxes was fixed and the temperature (300 K) was maintained by a Nosé-Hoover thermostat.[30] Then, a further 300 ps equilibration run was performed in the NPT ensemble using a Nosé−Hoover thermostat and barostat[30,31] with the temperature and the pressure fixed, respectively, at 300 K and 1 Bar. A second interfacial system, slightly larger than the one just described (cross section = 30 × 30 Å, with the water box containing 1200 water molecules and the HPT2 box containing 232 HPT2 molecules plus 21 water molecules), was obtained by the same procedure to execute the transfer of the larger TMA^+ ion.

The motion of the species was propagated in time via the Verlet velocity algorithm with a time step of 2 fs. Periodic boundary conditions were applied in all three directions, forming two liquid/liquid interfaces. Care was especially taken to confirm that the interfaces did not interact with each other.[16] To avoid interactions between the two interfaces, they must be separated by a substantial bulk region. In our simulation cell, the distance between the interfaces is 38 Å along the water phase and 61.68 Å along the HPT2 phase (i.e., 3.2 and 5.2 times greater than the long-range cutoff distance), which seems quite enough to avoid any interaction between the two interfaces. Long-range forces were calculated using the Ewald summation method with tinfoil boundary conditions. A molecular spherical cutoff of 12.25 Å (14.5 Å in the case of TMA^+) was applied to the real part of the Ewald energy. For the Lennard−Jones interactions, a cutoff of 10 Å was used. It is worth noting that the Ewald method can be used in the simulation of nonneutral systems if one includes a term corresponding to a background charge of opposite sign to the charge of the system, which makes the overall system neutral.[32−35] The forces between pairs at distances >10 Å were calculated by a multiple time step algorithm[36] with a integration step of 12 fs. Preliminary checks confirmed that good energy conservation (without thermostat) is achieved with this algorithm, and the system properties are unaffected by its use.

2. Free Energy Calculations. The best choice for the ion-transfer reaction coordinate is the distance of the ion to the interface. To calculate the corresponding PMF, a conventional constrained MD technique was employed.[37] The reaction coordinate was divided into slabs with a thickness of 5 pm. The ion was first kept fixed at the center of the first slab in bulk water phase, and its interactions were slowly turned on. After an equilibration run of 75 ps, the forces acting on the ion were averaged over a 2-ps trajectory. The ion was then put at the center of the next slab. A short 0.5-ps equilibration run was found to be enough to relax the solvent to the new position of the ion, considering the small ion displacement. Afterward, the forces acting on the ion were averaged again over a 2-ps trajectory. This procedure was repeated until the ion reached the bulk HTP2 phase. For each transfer, another independent PMF calculation was also performed in the reverse direction (i.e., from bulk HPT2 to bulk water), and the results presented correspond to the average of the two calculations. The results obtained in both directions were quite similar, and the hysteresis obtained lies inside the statistical uncertainties. Note that when the ion was in the organic phase, the averaging time in each slab was augmented to the double (1 ps of equilibration plus 4 ps of averaging), because of the slower rotational motion of the HPT2 molecules. This procedure led to total simulation times of 3500 ps for the alkaline ions, 5500 ps for the alkaline-earth ion, and 4500 ps for the organic ion. Some of the simulations proceeded a little bit further to confirm the convergence of the results, as discussed later. Similar strategies were successfully applied and proven to be very useful in the study of ion and

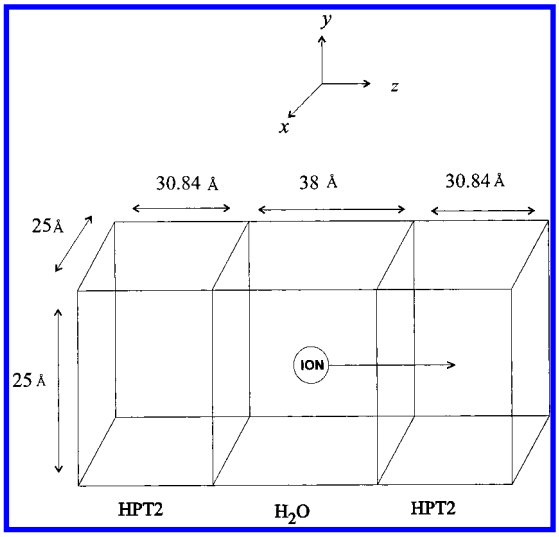

Figure 1. Schematic picture of the box used in the simulations.

neutral species transfer processes across liquid/liquid interfaces.[17,20,38,40]

The z axis of our internal frame was considered to be the axis perpendicular to the interfacial plane (see Figure 1). The free energy difference between a state where the ion is located at z_i and a reference state, z_{ref}, is given by[37,38,40]

$$\Delta G(z_i) = G(z_i) - G(z_{ref}) = -\int_{z_{ref}}^{z_i} \langle ||\vec{F}_z|| \rangle_{z'} dz' \qquad (3)$$

where $||\vec{F}_z||$ is the z component of the force acting on the ion and $\langle ... \rangle_{z'}$ represents NPT averages with the ion fixed in the z' position. In this paper, z_{ref} corresponds to the position of the ion in bulk water phase.

All simulations were carried out using the DL_POLY MD package.[41]

The statistical uncertainty associated with the calculation of the free energy of transfer was calculated by a block mean analysis. The data related to each transfer was divided into 10 statistically independent blocks. The results presented are the averages of the blocks, and the statistical uncertainties correspond to the root-mean-square of the results of the blocks. A similar procedure was employed to estimate the statistical uncertainties associated with the integration of the radial distribution functions.

III. Results

A. Potentials of Mean Force. The PMFs are crucial for a proper understanding of ion transfer processes, but they are innaccessible experimentally. It is in such cases that computer simulations become invaluable. In this section, the PMFs for all the ion transfers performed will be presented and analyzed.

Shown in Figure 2 are the PMF results obtained for several ion transfers. The shapes of these PMFs are all very similar, showing an increase in the Gibbs free energy as the ion moves from the water phase to the HPT2 phase. All the transfers appear to be nonactivated processes because no energy barriers are found. In the case of the Na^+ and Rb^+ ions, a very small energy barrier seems to arise in the organic phase at the end of the transfer. However, because its height is so close to the statistical uncertainty of the calculations, it may correspond to a small noisy oscillation in the free energy profile rather than to a real physical feature. When the ions are far from the interface and bulk conditions prevail, the free energy remains constant, showing that the reaction coordinate is fully examined. It should

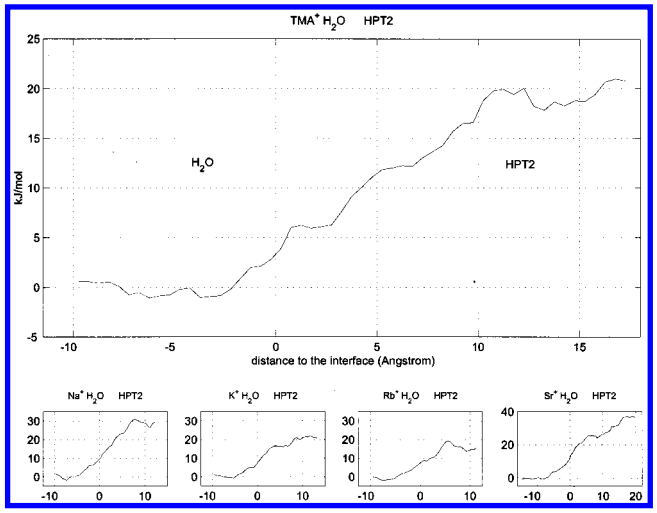

Figure 2. PMFs for the ion transfers. The ion being transferred is shown at the top of each plot. Units in the axis of the smaller plots are the same as the ones in the larger plot. Given the qualitative similarity between the free energy profiles, only one of them is shown with greater detail.

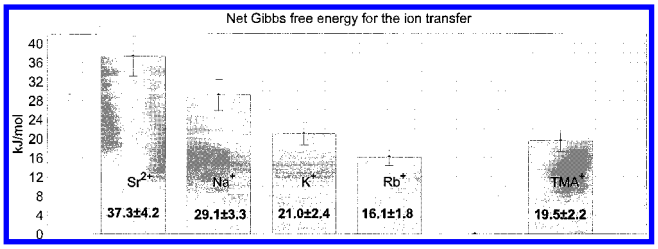

Figure 3. Net Gibbs free energy for the several ion transfer processes.

be said that the shapes of the PMFs in Figure 2 are quite similar to others already published.[17,18]

In contrast with the present results, Benjamin et al.[19] obtained a PMF that suggests an activated process for the transfer of Cl^- ion across the water/1,2-dichloroethane interface. In that pioneering work, the authors resorted to an approximate route for obtaining the PMF. In fact, they considered the free energy partitioned into independent Coulombic and Lennard Jones terms, thus neglecting any contributions coming from cross correlation terms. Because these cross terms may have non-negligible contributions,[42] without a more precise calculation it is not possible to confirm the exactness of the PMF obtained.

Our PMFs support the following picture for an ion transfer across the interface between two immiscible liquids. For this kind of process, the change in free energy is due to the exchange of the solvation shell of the ion. The major changes in the free energy only occur in the organic side of the interface. In the water phase, the slight increase of the free energy is mainly caused by the loss of water molecules of the second hydration shell of the ion and to the decrease of the long-range ion−solvent interactions when the ion is near the organic phase. In fact, the ion keeps its first solvation shell almost intact until it crosses the interface. The major contribution for the change in free energy associated with the transfer is the partial replacement, after crossing the interface, of the first hydration shell of the ion by HPT2 molecules.

For the transfer processes considered here, the net free energies obtained from the PMFs are depicted in Figure 3, together with the corresponding standard deviations calculated by a block means analysis.

Because all the experimental free energy values for the transfer of these ions were measured using other organic

TABLE 1: Free Energy of Ionic Solvation in Both Solvents (kcal/mol)[a]

ion	ΔG^{hyd}	ΔG^{solv} (SAT·HPT2)
Na^+	−98.5 (exp. −98.2)	−64.9
K^+	−80.9 (exp. −80.6)	−59.9
Rb^+	−75.5 (exp. −75.5)	−59.4
Sr_{2^+}	−345.9 (exp. −345.9)	−308.6

[a] The values for the free energy of hydration were taken from ref 39.

solvents, like the 1,2-dichloroethane or the nitrobenzene,[23,24] direct comparisons with our results would not be correct. Nevertheless, some simple observations can be made to check the accuracy of the present results. The free energy of the TMA^+ transfer (19.5 ± 2.2 kJ/mol) may be compared with the one (23.4 kJ/mol[21]) achieved by resorting to the theoretical model of Abraham and Linszi.[43,44] Good agreement is evident. On the other hand, the free energy for the transfer of the Rb^+ ion (16.1 ± 1.8 kJ/mol) is close to but smaller than the experimental value measured for the analogous I^- ion (21.9 kJ/mol[21]) using the same liquid/liquid interface. This result was to be expected because the stronger solvation of the cations by HPT2 contributes to the smaller value obtained for Rb^+. Indeed, the cations interact with the negative carbonyl oxygen but the anions cannot interact strongly with the positive carbonyl carbon that is too hidden by the methyl groups of the carbon chain. It is also important to note that the method employed here to calculate the free energy of transfer was applied before with the iodide ion, leading to good agreement with experimental data.[17] To get more quantitative detail into the energetics of the transfer process we can use the relation ΔG^{solv} (sat. HPT2) = $\Delta G^{hyd} - \Delta G^{transfer}$, which results from a simple thermodynamic cycle. Using the values for $\Delta G^{transfer}$ obtained here and the values of ΔG^{hyd} published by Åqvist[39] (using the same ion−water potentials and the same water model), we can calculate the free energy of ion solvation in saturated HPT2. The results are shown in Table 1.

The contribution of the water molecules in the H_2O/HPT2 mixed ionic solvation shells is specially important in the case of Sr^{2+}. As far as we know there are no experimental free energy values for the ion solvation in pure or saturated HPT2 published in the literature. However, we stress that Åqvist potentials were refined in solution to reproduce the experimental values for the free energy of hydration (as can be seen in the table). So, the reasonable results obtained for the free energy of transfer cannot result from any cancellation of errors but instead from a reasonable estimation of the free energy of solvation of the ion in saturated HPT2.

Finally, it should be noted that the experimental free energy dependence on the ion size and charge,[23,24] (i.e., $\Delta G^{w\to o}_{Sr^{2+}} > \Delta G^{w\to o}_{Rb^+}$ and $\Delta G^{w\to o}_{Na^+} > \Delta G^{w\to o}_{K^+} > \Delta G^{w\to o}_{Rb^+}$, is also correctly mirrored in our simulation results.

Further insight into the ion transfer process and its dependence on the ion size and charge should be gathered from the following section.

B. Exchange of the Ion's Solvation Shell. In this section, the dynamic process of the ion's solvation shell exchange, the water dragging effect, and the formation of water fingers are examined.

1. Radial Distribution Functions. An analysis of the ionic solvation as a function of the ion-interface distances was performed by looking at the corresponding radial distribution functions (RDFs). For that purpose, the simulation shell was divided into slabs parallel to the interface with a thickness of 2.5 Å, and the ion−water oxygen (O_w) and the ion−ketone oxygen (O_k) pair distribution functions were calculated independently in each slab. Then three-dimensional RDFs, functions of both the pair distance and the distance of the ion from the interface, were defined by a triangle-based linear interpolation technique. In the case of the TMA^+ ion, the RDFs were computed by considering its nitrogen atom as the center. Note that all RDFs were normalized by the corresponding bulk densities.

The ion−O_w RDFs are reported in Figure 4. For the alkaline ions, only the Na^+-O_w RDF is shown in this figure because all alkaline RDFs were very similar. In fact, the only remarkable difference between them is the decrease in the height of the first peak as the ions move toward the organic phase. That decrease, which is due to the dehydration of the first solvation shells of the ions, becomes clearly more marked as one goes from Na^+ to Rb^+, which will be discussed in detail next.

In Figure 4, one can observe that the first and the second peaks of the Na^+-O_w RDF become progressively smaller as the ion moves from water toward the organic liquid, because of the smaller number of water molecules hydrating this ion. However, even in the bulk organic phase, a partial hydration shell is retained, mainly its first shell, whereas its second shell almost disappears. In the case of the Sr^{2+} ion, its first hydration shell remains almost complete in the organic phase and a significant part of its second hydration shell is also retained. This result reflects the increased robustness of the hydration shells of the alkaline-earth ion, a consequence of its higher charge. In the case of the TMA^+ ion, the first solvation shell, which is broader than the ones of the monatomic ions, almost disappears in the organic phase. There is a slight increase at the end of the transfer that corresponds to the capture by the ion of one water molecule that was initially in the bulk organic solvent. The lower ability of the TMA^+ ion to retain its hydration shell is due to its more delocalized charge (+0.25 in each methyl group), that produces more, but weaker, interactions with the water molecules.

Figure 5 shows the RDFs for the ion−O_k pairs. Again only the RDF of one of the alkaline ions (i.e. the Na^+ ion) is shown for the same reasons as already discussed. One can observe the formation of two solvent shells around the Na^+ and the Sr^{2+} ions as they enter the organic phase, indicating the replacement of their hydration shells by the HPT2 molecules. The poorer statistics associated with the first peak in the $Sr^{2+}-O_k$ RDF is due to the very small number of HPT2 molecules in the first solvation shell of Sr^{2+}. Because the Sr^{2+} first hydration shell is almost complete, it is very difficult for the HPT2 molecules to reach it. With the increase of the fraction of HPT2 in the second shell, as this ion moves deeper into the organic phase, the HPT2 molecules may enter more easily from the second into its first solvation shell. The average number of HPT2 molecules in this ion first solvation shell converges to a value of 1.0. Such a reduced number explains the more noisy profile of the $Sr^{2+}-O_k$ RDF first peak.

In the case of the Na^+ ion, the first hydration shell is reduced to about half of its composition in bulk water and the HTP2 molecules have enough space to approach the ion, thus forming a well-defined first solvation shell. Due to its lower charge, the second solvation shell of the Na^+ ion (and of all the other alkaline metal ions) is much less pronounced than that of Sr^{2+}. Finally, in the case of the TMA^+ ion, one can notice the formation of a broad solvation shell due to the almost complete replacement of its hydration shell.

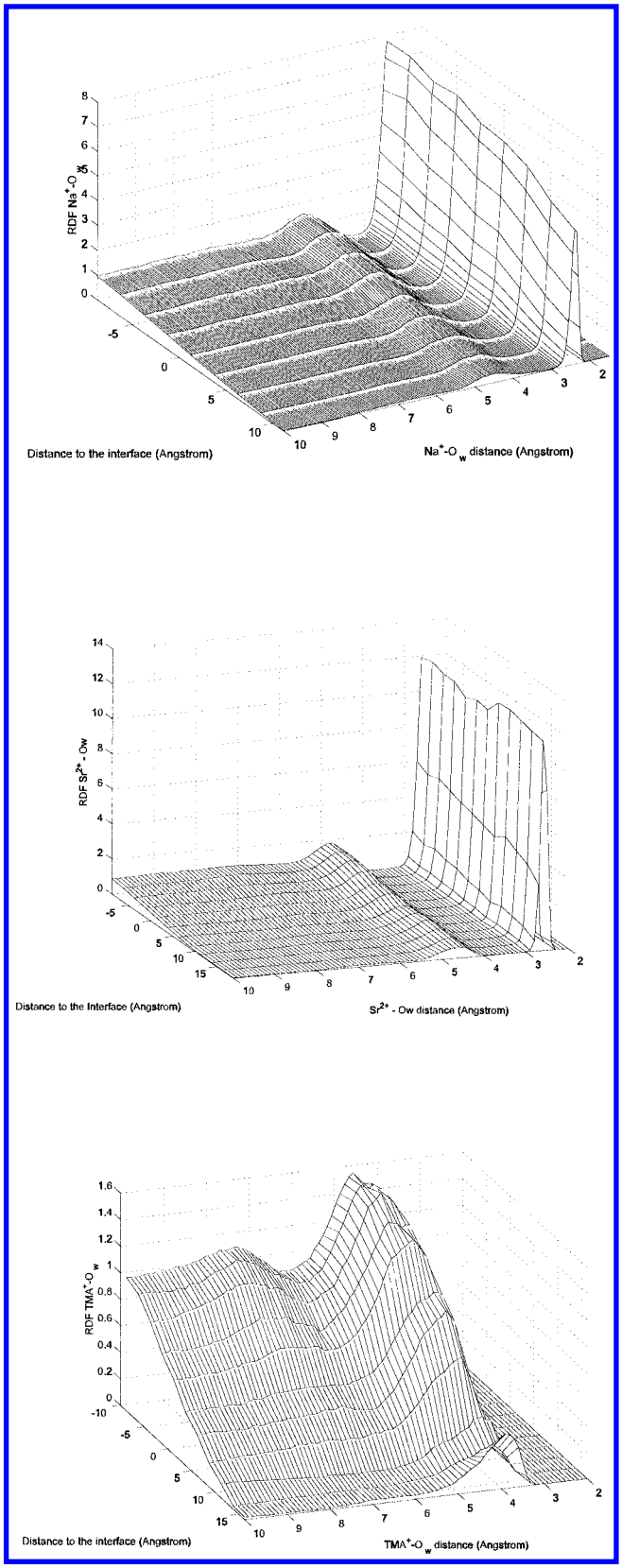

Figure 4. RDFs of the water oxygen (O_w) around the ions Na^+ (top), Sr^{2+} (middle), and TMA^+ (bottom) drawn as a function of the distance to the interface. Negative distance values correspond to the water phase and positive distance values correspond to the organic phase.

The solvation shell exchange is the key process for the ion transfer, so the RDFs were integrated to estimate the number of neighbors inside the ions first shells (and second shell for Sr^{2+}). These coordination numbers are depicted in Figure 6.

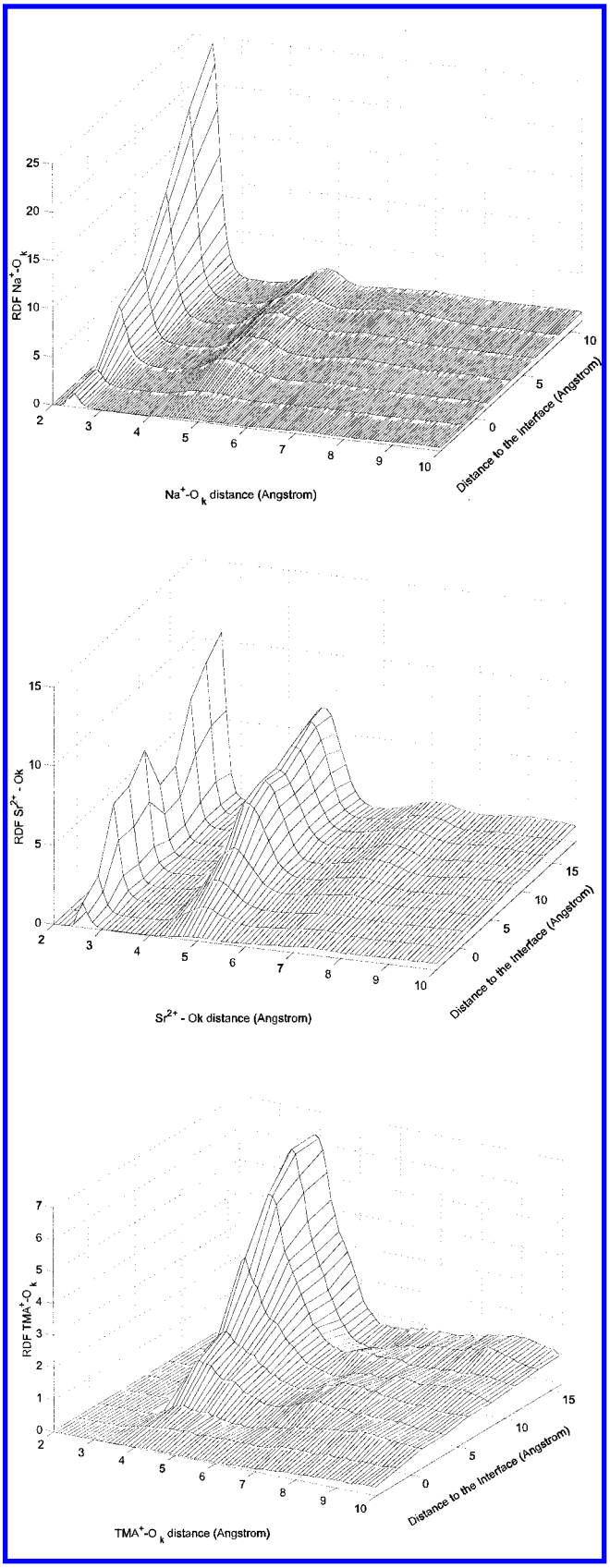

Figure 5. RDFs of the ketone oxygen (O_k) around the ions Na^+ (top), Sr^{2+} (middle), and TMA^+ (bottom) drawn as a function of the distance to the interface. Negative distance values correspond to the water phase and positive distance values correspond to the organic phase.

At this point it is important to clarify that some tests were made to check the convergence of the present results. The simulation of the K^+ transfer process was extended to enable a

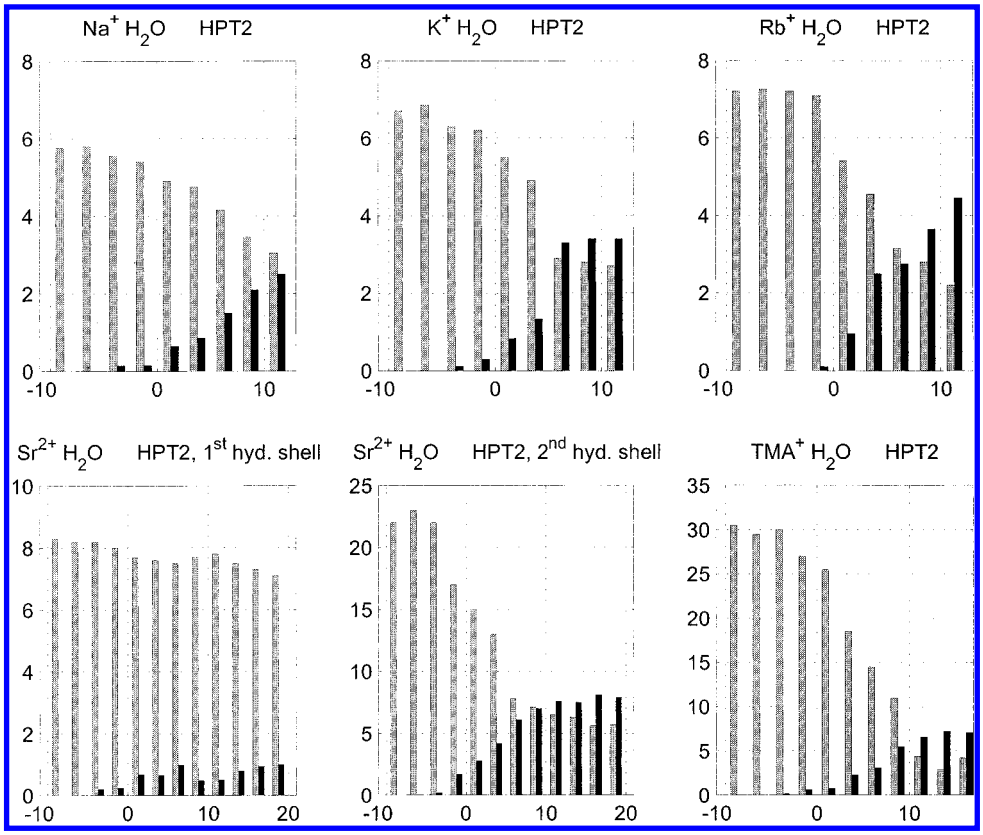

Figure 6. Coordination numbers for the first solvation shells of the several ions as a function of the distance to the interface. In the case of the Sr^{2+} ion, the coordination numbers for the second solvation shell are also shown. Black bars correspond to the number of HPT2 molecules and the gray bars correspond to the number of water molecules.

deeper penetration of the ion (10 Å more) into the organic phase. This procedure was done to confirm that the free energy and the composition of its solvation shell remained constant. A series of simulations was also performed starting with each ion in a large box ($30 \times 30 \times 45$ Å^3) filled with HTP2 saturated with water. At the beginning of the simulation the ions were completely unhydrated. However, during an equilibration of 250 ps, the ions captured some water molecules (that were initially solvated in HPT2) into their solvation shells (2−3 for the alkaline ions, 11 for Sr^{2+}, and 4 for TMA^+). After establishing those mixed solvation shells, the composition of the solvation shell of the ions remained constant, showing that an equilibrium situation was achieved. It should be noticed that the HPT2 saturated with water contains 8.3% (mol/mol) of water. Such a high concentration of water allows the ions to keep half-hydrated in the organic solvent in a equilibrium state. The composition of the solvation shells of the ions at the end of the transfer to the organic solvent was the same (within statistical uncertainty) as the one resulting from the equilibration of the ions in saturated HPT2. Thus, it can be concluded that the final state of the ions after the transfer does indeed correspond to the final state of the transfer reaction, and the ions will keep the water molecules in their solvation shells in saturated HPT2 even on a longer time scale.

Finally, it should be stressed that this conclusion is only valid for HPT2 because of the high solubility of water in this solvent. In very hydrophobic solvents, like 1,2-dichloroethane or nitrobenzene, the water solubility is almost null. Thus, the final state of the transfers can eventually be very different regarding the maintenance of mixed solvation shells.

2. Water Dragging Effect. The transportation by the ions of water molecules into the organic phase (the so-called water dragging effect) revealed in the simulations is in fair agreement with experimental findings. It is well-known that the water content in the organic phase increases with the transfer of ions. Water coextraction was detected using several organic solvents, such as nitrobenzene, either pure or in mixtures with benzene, 4-methyl-2-pentanone, or chloroform.[24,45−53] In some cases, accurate numbers of coextracted molecules could be experimentally measured.[24,49−53] Using nitrobenzene as the organic solvent, the more recent values for the number of coextracted water molecules[24] from Na^+ to Rb^+ ranged from 3.8 to 0.7, and a value of 14 ± 2 water molecules coextracted by Ca^{2+} was obtained. In the present simulations, the summation of the water molecules dragged into the organic phase in the first and second hydration shells of Sr^{2+} is estimated at 13 ± 1. In the case of TMA^+, no water coextraction into nitrobenzene was detected. In the present work, the TMA^+ ion was the one that dragged the smallest fraction of its hydration shell into HPT2 (∼10% of the water molecules that were hydrating the ion in bulk water phase). Although direct quantitative comparison with our system would not be correct, the closeness of the simulation results to those experimental measurements confirms that the magnitude of the effect obtained in the simulations is correct. The slightly higher number of coextracted molecules in the simulated system reflects the greater hydrophilicity of HPT2 compared with nitrobenzene.

A last very simple and interesting analysis consists of calculating the fraction of the hydration shell retained by the ions as they progress into the organic solvent. This quantity can be simply defined as:

$$\chi_{\text{h·shell}}(z) = \frac{n^{\text{o}}\text{H}_2\text{O}(z)}{\langle n^{\text{o}}\text{H}_2\text{O}\rangle_{\text{bulk}}} \qquad (4)$$

where $\chi_{\text{h·shell}}$ corresponds to the z-dependent fraction of the

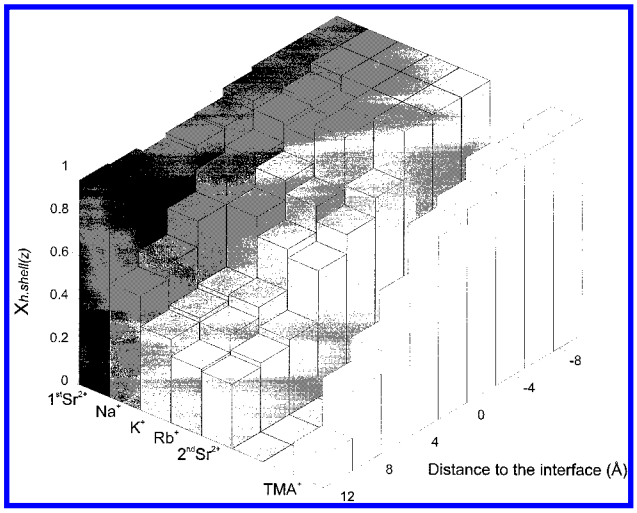

Figure 7. Fraction of the hydration shell conserved by the ions as a function of the distance to the interface. In the case of Sr^{2+}, the results shown include the first and the second hydration shells.

hydration shell, $n^oH_2O(z)$ is the number of water molecules in the hydration shell of the ion given that the ion is in the z position, and $\langle n^oH_2O\rangle_{bulk}$ corresponds to the bulk average number of water molecules in the hydration shell of the ion. The results are depicted in Figure 7. Observing Figure 7, the relative robustness of the ion's hydration shells, and the effect of the ion's size and charge under the magnitude of the exchange of the solvation shell become quite clear. Data relative to TMA^+ was spaced by a gap to remember that it should not be directly compared with the monatomic ions because several differences are simultaneously present (ion size, charge deslocalization, ion shape, etc.). It is interesting to compare these results with the predictions of the model of Sanchez et al.[23] for the transfer of ions across liquid/liquid interfaces, which explicitly takes into account the transfer of hydrated ions into the organic phase. Although the theory was developed considering the transfer of the ion with a complete (and not partial) hydration shell, its basic conclusions based on thermodynamic considerations (i.e., that the transfer of hydrated ions "should be favored in the case of highly charged small ions at interfaces with a relatively low surface tension and large differences between the reciprocal of the dielectric constants.") are fully confirmed here with regard to the ion's size and charge. The dependence on the organic solvent falls beyond the scope of this work.

3. Formation of Water Fingers. Observing the animated trajectories of the simulations we can see that as the ions cross the interface and move toward the organic phase they remain connected to the water phase through a water chain. That water chain resists until the distance of the ion from the aqueous phase reaches >10 Å from the water phase (14 Å in the case of Sr^{2+}), after which the water finger disrupts and retracts. The same phenomenon was also observed in the reverse transfer, from the HPT2 phase to water. As the ions approach and get close enough to the water phase, a water capillary wave penetrates into the organic phase and becomes connected to the ion. These kinds of structures were also observed in other ion transfer simulations[17,19] and are a result of the balance between the more favorable ion−water interactions and the replacement of a part of the water−water interactions for the water molecules in the water finger by the less energetic water−HPT2 interactions. Figure 8 shows two water fingers in its maximum extension, before disruption and retraction, formed during the transfer of Rb^+ and Sr^{2+} into the organic phase.

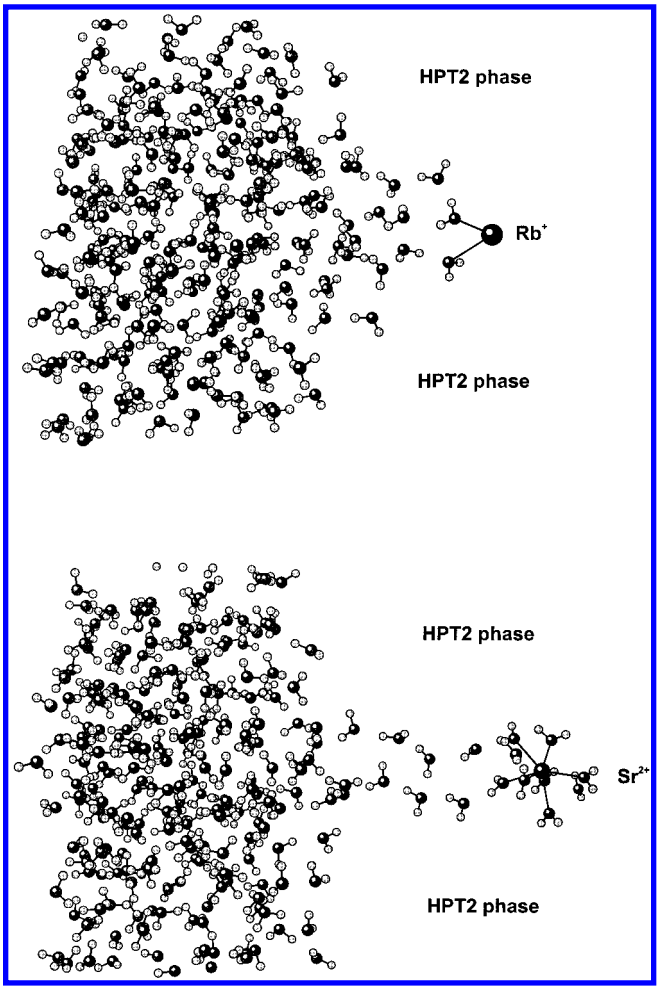

Figure 8. Snapshot of two water cones of different extension protruding into the HPT2 phase to solve the Rb^+ and Sr^{2+} ions. For clarity, the HPT2 molecules were deleted.

In the present simulations the extent of the water fingers was basically insensitive to the size of the ion (it was statistically the same for the organic and for all the alkaline ions), but quite sensitive to the charge of the ion because, as in the case of the alkaline-earth ion, the water finger was significantly longer. The explanation for this behavior should rely on the difference between the long-range interactions of the ions with water. Hence, the capacity of all monocharged ions to interact with the water molecules of the water finger beyond their first hydration shell is quite similar, because they all have the same charge and the dispersive term, which is different for all them, is short-ranged. The Sr^{2+} ion, however, has a much superior capacity to attract more distant water molecules, because of its higher charge, that better stabilizes the water finger structure. The simple observation of the more pronounced second hydration shell of Sr^{2+}, compared with the ones of the alkaline ions, illustrates this idea and justifies the larger extension of the water finger obtained with this ion.

Figure 9 represents the probability distribution for the angle between the water dipole moment and the z axis of our internal frame as a function of the distance to the interface. The two interfaces are located at $z = 0$ Å and $z = -40$ Å. The ion, as illustrated in Figure 8, is located at $z = 14$ Å (14 Å deep into the organic phase) and is connected to the water phase through a water chain, just before disruption. In bulk water phase, the orientational distribution is uniform as it should be for an isotropic liquid. At $z = -40$ Å, the existence of the liquid/

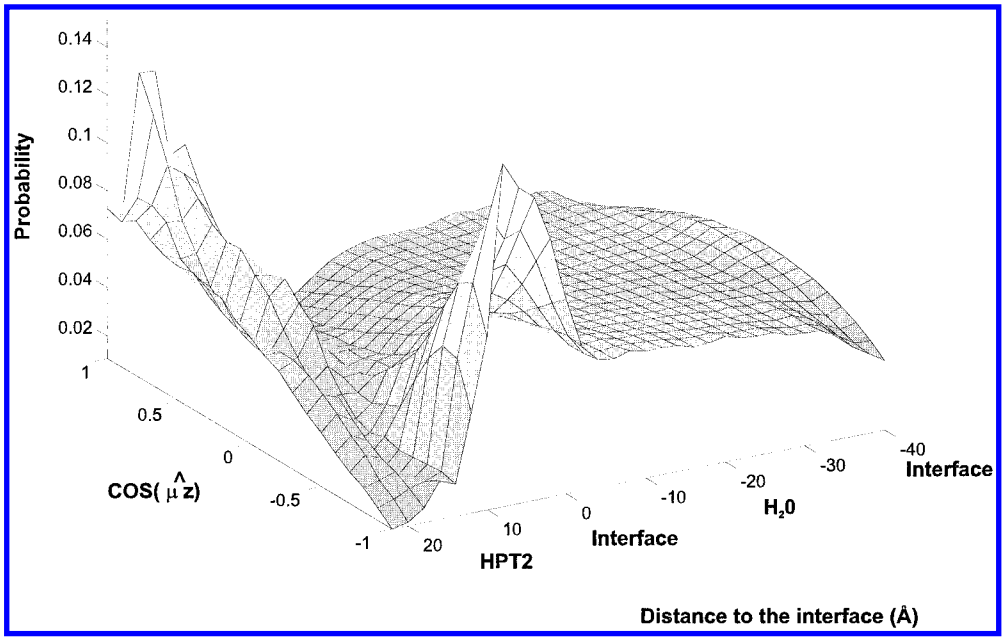

Figure 9. Distribution of the cosine of the angle between the water dipole moment and the *z* axis of the internal frame as a function of the distance to the interface, given that the Sr^{2+} ion is located at $z = 14$ Å and connected to the water phase by a water finger.

liquid interface causes an preferential orientation of the dipole moments parallel to the interfacial plane ($\cos(\widehat{uz}) = 0$), an effect previously documented in literature (see ref 16). A broad peak appears between $z = -2$ Å and $z = 14$ Å, with $\cos(\widehat{uz}) = -1$, which means that the water dipole moments exhibit a preferential orientation parallel to the *z* axis and pointing in the opposite direction of the ion. The second peak beginning at $z > 14$ Å, with $\cos(\widehat{uz}) = 1$, refers to the water molecules inside the Sr^{2+} hydration shell located deeper than the ion in the organic phase. This peak also indicates a preferential orientation parallel to the *z* axis that also points in the opposite direction of the ion. This picture confirms the long-range polarization of the water molecules in the water finger by the Sr^{2+} ion.

IV. Conclusions

This work reports studies of the transfer of several alkaline ions (Na^+, K^+, and Rb^+), an alkaline-earth ion (Sr^{2+}), and an organic ion (TMA^+) across the water/HPT2 interface by MD simulations. The PMFs were calculated for all those ion transfers. In addition, the dynamics process of the ion's solvation shell exchange, the water dragging effect and the water finger phenomenon were analyzed from a microscopic perspective. The calculated PMFs revealed a monotonic increase in the free energy as the ion leaves the water phase and enters into the organic phase. No energy barriers were found for these transfer processes and, therefore, they seem to be activationless. The greatest changes in the free energy only happen after the ion crosses the interface and are due to the partial exchange of the ion's first solvation shell. The net free energy for the transfers exhibits a dependence on the ion's size and charge, decreasing with the increase of the size of the ion ($\Delta G_{Na^+}^{w\to o} > \Delta G_{K^+}^{w\to o} > \Delta G_{Rb^+}^{w\to o}$) and with the decrease of the charge of the ion ($\Delta G_{Sr^{2+}}^{w\to o} > \Delta G_{Rb^+}^{w\to o}$). This result is corroborated by experimental work performed with other liquid/liquid interfacial systems. From the analysis of the process of the exchange of the ion's solvation shell, it has been demonstrated that when the ions progress from water toward the interface they keep their first hydration shell almost unaffected. Only after crossing the interface does the process of exchange of the solvation shell extensively occur. After crossing the interface, the exchange of the second hydration shell of the organic and all the alkaline ions is almost complete, although Sr^{2+} ion still retains ~25% of its second hydration shell because of its higher charge. Regarding the first hydration shell, it is only partially exchanged in an extension that depends on the ion's size and charge. The replacement of the solvation shells of the ions is fulfilled when the ions penetrate deeper than ~12 Å (17 Å for the Sr^{2+} ion) into the organic phase. All the ions in the organic phase remain connected to the water phase through a water chain when their distance from the interface is <10 Å. For the Sr^{2+} ion, this distance was 14 Å; this difference is caused by the stronger long-range interactions of the Sr^{2+} ion with the water molecules that better stabilize the water finger structure. As the ions penetrate even deeper into the organic phase, the water chain disrupts and retracts. The simulations also revealed that a fraction of the hydration shell is retained by the ions in the organic phase, forming a mixed H_2O/HPT2 solvation shell and mirroring the experimentally well-known water dragging effect. The fraction of the hydration shell transferred into the organic phase increases with the increase of the ionic charge and the decrease of the ionic size, in accord with the recent theoretical model of Sanchez et al.[23] The number of coextracted molecules also seems to be in fair agreement with other similar experimental studies that employ other organic solvents.

Acknowledgment. Financial support from Fundação para a Ciência e a Tecnologia (Lisbon) through project PRAXIS/2/2.1/QUI/474/94 is acknowledged. P. A. F. thanks the Programa Praxis XXI for a doctoral scholarship (BD/9175/96). The authors have benefited from valuable discussions with Prof. António F. Silva and Alfredo J. P. Carvalho.

References and Notes

(1) Cunnane, V. J.; Schiffrin, D. J.; Beltran, C.; Geblewicz, G.; Solomon, T. *J. Electroanal. Chem.* **1988**, *247*, 203.

(2) Koryta, J.; Skalicky, M. *J. Electroanal. Chem.* **1987**, *229*, 265.

(3) Arai, K.; Ohsawa, M.; Kusu, F.; Takamura, K. *Bioelectrochem. Bioenerg.* **1993**, *31*, 65.

(4) Higgins, D. A.; Corn, R. M. *J. Phys. Chem.* **1993**, *97*, 489.

(5) Grubb, S. C.; Kim, M. W.; Rasing, T.; Shen, Y. R. *Langmuir* **1988**, *4*, 452.

(6) Conboy, J. C.; Daschbach, J. L.; Richmond, G. L. *J. Phys. Chem.* **1994**, *98*, 9688.
(7) Du, Q.; Superfine, R.; Freysz, E.; Shen, Y. R. *Phys. Rev. Lett.* **1993**, *70*, 2313.
(8) Eisenthal, K. B. *Annu. Rev. Phys. Chem.* **1992**, *43*, 627.
(9) Shen, I. N. *Annu. Rev. Phys. Chem.* **1989**, *40*, 327.
(10) Mitrinovic, D.; Zhang, Z.; Williams, S.; Huang, Z.; Schlossman, M. *J. Phys. Chem. B* **1999**, *103*, 1779.
(11) Lynse, P. *J. Chem. Phys.* **1987**, *86*, 4177.
(12) Gao, J.; Jorgensen, W. *J. Phys. Chem.* **1988**, *92*, 5813.
(13) Benjamin, I. *J. Chem. Phys.* **1992**, *97*, 1432.
(14) Michael, D.; Benjamin, I. *J. Phys. Chem.* **1995**, *99*, 1530.
(15) Chang, T.; Dang, L. X. *J. Chem. Phys.* **1996**, *104*, 6772.
(16) Fernandes, P. A.; Cordeiro, M. N. D. S.; Gomes, J. A. N. F. *J. Phys. Chem. B* **1999**, *103*, 6290.
(17) Fernandes, P. A.; Cordeiro, M. N. D. S.; Gomes, J. A. N. F. *J. Phys. Chem. B* **1999**, *103*, 8930.
(18) Benjamin, I. *J. Chem. Phys.* **1992**, *96*, 577.
(19) Schweighofer, K.; Benjamin, I. *J. Phys. Chem.* **1995**, *99*, 9974.
(20) Lauterbach, M.; Engler, E.; Muzet, N.; Troxler, L.; Wipff, G. *J. Phys. Chem. B* **1998**, *102*, 245.
(21) Cheng, Y.; Schiffrin, D. *J. Electroanal. Chem.* **1996**, *409*, 9.
(22) Cheng, Y.; Schiffrin, D. *J. Electroanal. Chem.* **1997**, *429*, 37.
(23) Sanchez, C.; Leiva, E.; Dannie, S.; Baruzzi, A. *Bull. Chem. Soc. Jpn.* **1998**, *71*, 549.
(24) Osakay, T.; Ogata, A.; Ebina, K. *J. Phys. Chem.* **1997**, *101*, 8341.
(25) Berendsen, H. J. C.; Postma, J. P. M.; van Gunsteren, W. F.; Hermans, J. In *Intermolecular Forces*; Pullman, B., Ed.; Reidel: Dordrecht, 1981; p 331.
(26) Ryckaert, J.; Ciccotti, G.; Berendsen, H. *J. Comput. Phys.* **1977**, *23*, 327.
(27) Brooks, B. B.; Bruccolery, R. E.; Olafson, B. D.; States, D. J.; Swaminathan, S.; Karplus, M. J. *J. Comput. Chem.* **1983**, *4*, 187.
(28) Fernandes, P. A.; Cordeiro, M. N. D. S.; Gomes, J. A. N. F. *J. Phys. Chem. B* **1999**, *103*, 1176.
(29) Pearlman, D. A.; Case, D. A.; Cadwell, J. C.; Seibel, G. L.; Sing, U. C.; Weiner, P.; Kollman, P. A. *AMBER4*; University of California: San Francisco, 1991.
(30) Hoover, W. G. *Phys. Rev.* **1985**, *A31*, 1695.
(31) Melchionna, S.; Ciccotti, G.; Holian, B. L. *Mol. Phys.* **1993**, *78*, 533.
(32) Roberts, J. E.; Schnitker, J. *J. Chem. Phys.* **1994**, *101*, 5024.
(33) Figueirido, F.; Buono, G. S. D.; Levy, R. M. *J. Chem. Phys.* **1995**, *103*, 6133.
(34) Wasserman, E.; Rustad, J.; Xantheas, S. *J. Chem. Phys.* **1997**, *106*, 9769.
(35) Mart'nez, J.; Pappalardo, R.; Sánchez-Marcos, E.; Refson, K.; D'az-Moreno, S.; Muñoz-Páez, A. *J. Phys. Chem. B* **1998**, *102*, 3272.
(36) Forrester, T. W.; Smith, W. *Mol. Simul.* **1994**, *13*, 195.
(37) Paci, E.; Ciccotti, G.; Ferrario, M.; Kapral, R. *Chem. Phys. Lett.* **1991**, *176*, 581.
(38) Chang, T.; Dang, L. X. *J. Chem. Phys.* **1998**, *108*, 2.
(39) Åqvist, J. *J. Chem. Phys.* **1990**, *94*, 8021.
(40) Meyer, M.; Hayoun, M.; Turq, P. *J. Phys. Chem.* **1994**, *98*, 6626.
(41) Forrester, T. W.; Smith, W. *DLPOLY* (*2.1 version*); CCLRC: Daresbury Laboratory, Daresbury, UK, 1995.
(42) van Gusteren, W.; Mark, A. *J. Chem. Phys.* **1998**, *108*, 6109.
(43) Abraham, M. A.; Namor, A. F. D. D. *J. Chem. Soc., Faraday Trans.* **1976**, *72*, 955.
(44) Abraham, M. A.; Liszi, J. *J. Inorg. Nucl. Chem.* **1981**, *43*, 143.
(45) Kenjo, T.; Diamond, R. *J. Phys. Chem.* **1972**, *76*, 2454.
(46) Kenjo, T.; Diamond, R. *J. Inorg. Nucl. Chem.* **1974**, *36*, 183.
(47) Kusakabe, S.; Shinoda, M.; Kusafuka, K. *Bull. Chem. Soc. Jpn.* **1989**, *62*, 333.
(48) Kusakabe, S.; Arai, M. *Bull. Chem. Soc. Jpn.* **1996**, *69*, 581.
(49) Rais, J.; Kyrs, M.; Pivonková, M. *J. Inorg. Nucl. Chem.* **1968**, *30*, 611.
(50) Motomizu, S.; Tôei, K.; Iwashido, T. *Bull. Chem. Soc. Jpn.* **1969**, *42*, 1006.
(51) Kawasaki, M.; Tôei, K.; Iwashido, T. *Chem. Lett.* **1972**, 417.
(52) Iwashido, T.; Minami, M.; Kimura, M.; Sadakani, A.; Kawasaki, M.; Tôei, K. *Bull. Chem. Soc. Jpn.* **1980**, *53*, 703.
(53) Yamamoto, Y.; Tarumoto, T.; Tarui, T. *Chem. Lett.* **1972**, 459.